González Buch, C.; Herraiz Cardona, I.; Ortega Navarro, EM.; García Antón, J.; Pérez Herranz, V. (2016). Study of the catalytic activity of 3D macroporous Ni and NiMo cathodes for hydrogen production by alkaline water electrolysis. Journal of Applied Electrochemistry. 46(7):791-803. doi:10.1007/s10800-016-0970-0.

Study of the Catalytic Activity of 3D Macroporous Ni and NiMo Cathodes for Hydrogen Production by Alkaline Water Electrolysis

C. González-Buch, I. Herraiz-Cardona, E. Ortega, J. García-Antón, V. Pérez-Herranz*

Ingeniería Electroquímica y Corrosión (IEC), Departamento de Ingeniería Química y Nuclear, Universitat Politècnica de València. Camí de Vera, s/n. 46022 Valencia, Spain

*Corresponding author. Tel.: +34-96-3877632; fax: +34-96-3877639;

E-mail address: vperez@iqn.upv.es (V. Pérez-Herranz)

Abstract

Platinum is the electrode material with the highest catalytic activity for the hydrogen evolution reaction (HER). However, its high cost and scarcity are the two major barriers for its usage in the industrial alkaline water electrolysis, which requires searching for other cheaper and more available materials with good catalytic activity. Ni-based materials have attracted more and more attention due to their good activity for the HER and sufficient corrosion resistance in alkaline solutions at considerable low cost. According to the Brewer intermetallic bonding theory, molybdenum alloyed with nickel (hypo-hyper-d-electronic transition metal) could improve the intrinsic catalytic activity for the HER.

In this work, Ni and NiMo metallic coatings were galvanostatically electrodeposited on a stainless steel AISI 304 substrate by means of the double-template electrochemical process. The evaluation of these electrodes as H_2-envolving cathodes was done in 30% wt. KOH by pseudo-steady-state polarization curves and electrochemical impedance spectroscopy (EIS) at different temperatures. From Tafel curves results, it is shown that the NiMo electrodes have higher catalytic activity than Ni. On the other hand, from EIS results, it is possible to conclude that the NiMo electrodes showed higher intrinsic

catalytic activity for HER than the pure Ni electrode as a consequence of alloying hypo-hyper-d-electronic transition metals.

Keywords: NiMo alloys, HER, Surface Roughness factor, catalytic activity, alkaline water electrolysis.

1. Introduction

As an alternative to fossil fuels, hydrogen is considered one of the most promising energy carriers for the future because it is versatile, environmentally compatible and it could be produced from renewable energy sources [1-3]. There are several methods to produce hydrogen, but alkaline water electrolysis is one of the most promising methods for clean and renewable hydrogen production [4-6]. However, its high cost, both economic and energetic, restrains the use of this technique for hydrogen large-scale production [4]. This cost is directly proportional to the operating voltage, which depends on the overpotential of the oxidation and reduction reactions taking place at the anode and cathode respectively. That is why the effort in developing new cathode materials with lower overpotential for the hydrogen evolution reaction (HER) reduces the cost of energy from hydrogen production by electrolysis [7].

The optimum electrode material for HER must combine strong catalytic activity, large surface area, stability of performance and low cost [8]. Platinum is the electrode material with the highest catalytic activity for HER. However, its high cost and scarcity are the two major barriers for its usage in the industrial water electrolysis, which requires searching for other cheaper and more available materials with good catalytic activity [4, 9, 10]. Ni-based materials have attracted more and more attention due to their good activity for HER and sufficient corrosion resistance in alkaline solutions at considerable low cost [10-13]. In order to improve the intrinsic catalytic activity, binary or ternary catalytic systems have been deeply studied such as: NiCo [14-18], NiFe [19-22], NiW [19,23], NiCu [24], NiAl [25], NiZn [26,27].

According to the Brewer intermetallic bonding theory [28], when metals of the left half of the transition series in the periodic table with empty or less-filled d-orbitals are alloyed with metals of the right half of the series with more filled d-bands, a

maximum in bond strength and stability of the intermetallic alloy phases is expected [28], there is a well-pronounced synergism in the electrocatalysis [29-30]. The d-orbital participates in both the lattice and the chemisorptive bond, so when two hypo-hyper-d-electronic transition metals mutually interact, changes in catalytic activity are expected. This synergistic effect often exceeds the effects of the individual parent metals and approaches reversible behavior, it is they can be used both as cathodes and anodes, within a wide range of current densities [28,31-32].

As it has been mentioned, nickel and nickel based alloys have been widely studied as cathodes for HER. Among these materials, NiMo has particularly high catalytic activity [23,25,33-41].

The aim of the present work is the development of 3D macroporous Ni and NiMo electrodes in order to evaluate their suitability for the HER in terms of catalytic activity. The developed electrodes were characterized morphologically by confocal laser scanning microscopy, SEM and EDX; and electrochemically in 30 wt.% KOH solution by means of pseudo-steady-state polarization curves and electrochemical impedance spectroscopy (EIS).

2. Experimental

2.1. Preparation of electrodes

The metallic coatings were galvanostatically electrodeposited on a stainless steel AISI 304 substrate with a cross-sectional available area of 0.5 cm^2 previously pretreated to guarantee an adherent deposit. The pretreatment consists in an initial roughing down and polishing with silicon carbide emery paper with different grits (220, 500, 1000 and 4000) to a mirror surface finish. Then the electrode surface was degreased by immersing it in 25 wt.% NaOH at 90 °C for 1 minute and stripped by immersing it, in this case, in 18 wt.% HCl at room temperature for 1 minute. This was followed by an anodic treatment in 70 wt.% H_2SO_4 for 3 minutes at a current density of 1080 A m^{-2} [42], and finally a cathodic treatment in a solution of 240 g L^{-1} of $NiCl_2$ and 125 mL L^{-1} HCl at room temperature for 5 minutes at a current density of 269 A m^{-2}, the aim of this step is to produce a thin, adherent deposit of nickel which serves as a base for the subsequent electrodeposition [43]. Between each treatment and before the electrodeposition, the electrode was washed with distilled water.

The formation of electroactive coatings was done via a double-template electrochemical process described in our previous works [44,45]. By means of this process is possible to obtain self-supported nanoramified (denditric) deposits in a simple way. It consists of an electrochemical deposition which takes place simultaneously with the hydrogen evolution. The hydrogen bubbles generated in highly acidic media and at high cathodic current densities function as a dynamic template during Cu deposition. The resulting structures are 3D foams of Cu with highly porous ramified (denditric) walls. Afterwards the Cu macroporous layer acted as a template for the nickel and nickel-molybdenum deposition. Table 1 summarizes the bath composition and deposition conditions for the fabrication of the electroactive coatings. As it can be seen

from this Table, three different electrocatalysts have been developed. The Ni electrode was obtained onto a Cu template electrodeposited from a bath containing $CuSO_4$, H_2SO_4 and HCl. It has been shown [46] that HCl addition decreases the size and the agglomeration of the branches which form the wall of the foam, resulting in a larger specific surface area. This is because the chloride ions catalyze the reduction of copper [47-49]. Even a trace amount of chloride ion in the solution would change the reaction mechanism for the electron transfer from the outer-sphere reaction (water-water bridge) to inner-sphere reaction (chloride bridge), resulting in much higher exchange current density of the Cu^{2+}/Cu^{+} reaction step [46]; and therefore the foam wall is more effectively filled with copper deposits. Two different NiMo electrodes have been developed, however in this case, adding HCl to the electrodeposition bath to obtain the copper template made the subsequent deposits of NiMo alloy be not enough adherent. Therefore, the template was performed without the presence of chloride ions. The electrodeposition bath was the same for both NiMo developed electrodes [50] and the only difference in the operating conditions between the NiMo1 and NiMo2 electrodes was the time of the NiMo electrodeposition. 30 minutes were been employed to obtain the NiMo1 electrocatalyst and 60 minutes for the NiMo2.

Figure 1a shows the cell used for the electrodeposition process. In this thermostated one-compartment cell, the substrate surface to be coated is placed in horizontal "face-up" position, allowing the free release of the generated gas bubbles. The counter electrode was a 0.57 cm^2 surface area platinum electrode. The reference electrode was a commercially available Ag-AgCl (3 M KCl electrolyte) electrode. The electrodepositions were carried out by using an AUTOLAB PGSTAT302N potenciostat/galvanostat.

The surface morphologies and compositions of the developed electrocatalytic coatings were studied by means of an OLYMPUS LEXT OLS3100-USS confocal laser scanning microscope, and a ZEISS ULTRA 55 field emission scanning electron microscope (FE-SEM) coupled with an Energy-Dispersive X-Ray (EDX) analysis.

2.2. Electrochemical measurements

The evaluation of these electrodes as H_2-envolving cathodes was done in 30 wt.% KOH by pseudo-steady-state polarization curves and electrochemical impedance spectroscopy (EIS) at different temperatures: 30, 40, 50, 60, 70 and 80 ºC. The operating conditions were described in our previous works [14,17,18].

The electrochemical measurements were carried out in the electrochemical cell P200002526 [51] showed in Figure 1.b. In this cell, the developed electrocatalysts were used as the working electrodes, placing the electrode/electrolyte interface in a vertical plane, in order to allow the free evolution of the produced hydrogen bubbles when necessary. In this case, the counter electrode was a large-area Ni foam produced from 0.17 cm thick INCOFOAM^{TM} sheets, with 50 pores per linear inch. The reference electrode and the potenciostat/galvanostat were the same which were used in the electrodeposition process.

3. Results and discussion

3.1. Morphology and composition of the electrodes

Figure 2 shows the field emission scanning electron microscopy micrographs of the developed electrocatalysts at low (Fig. 2a, 2d and 2g) and high (Fig. 2b, 2e, and 2h) magnifications; and 3D confocal laser microscopy micrographs (Fig. 2c, 2f and 2i). As it can be seen from Fig. 2a, the Ni electrode presents a 3D foam structure whose walls are composed of a large number of small-ramified branches (Fig. 2b). This type of macrostructure is obtained because of the electrodeposition of Cu occurs simultaneously with hydrogen generation, so that the sites where bubbles of H_2 are generated there is no metal available for electrodeposition, forming pores with different sizes which depend on the size of the hydrogen bubbles. In the Ni electrode, that size is around 120-220 μm.

From the NiMo1 micrographs it can be shown that only 30 minutes of electrodeposition onto the Cu template structure are enough to lead to a different macrostructure. The pores are not completely defined (Fig. 2d) and the branches of the walls of the 3D foam structure are further bonded (Fig. 2e). If we increase the time of electrodeposition of NiMo up to an hour (Electrode NiMo2) the macrostructure obtained (Fig. 2g) is more similar to the one obtained with the Ni electrode but the branches will show less order and smaller size of the pores, obtaining, as much, pores of 150 μm.

Table 2 shows the composition of the investigated electrocatalytic coatings in at.% obtained by means of EDX analysis coupled to the FE-SEM. As it can be observed, increasing the electrodeposition time from 30 to 60 minutes, the amount of Mo in the deposit increases, reaching a 14.3 at.%. The copper used as a template for the coating of Ni-Mo is not detected by EDX analysis indicating that the Cu template is

completely covered by the Ni-Mo alloy. This is interesting as the aim of this work is to evaluate the catalytic activity towards the HER of the NiMo cathodes.

3.2. Polarization measurements

Figure 3a shows the Tafel polarization curves obtained in 30 wt.% KOH for the developed electrocatalysts at 30 ºC (filled dots) and 80 °C (empty dots). The curves were corrected with respect to the equilibrium potential for the HER and the ohmic drop. As it can be observed, the catalytic activity increases with the temperature because the kinetic of the reaction improves with this parameter. The curves exhibit the classic Tafel behavior, indicating that the HER on these electrodes is purely kinetic controlled and can be described by the Tafel equation, $\eta = a + b\log j$, where η (V) represents the overpotential responsible of the cathodic current density j (A cm^{-2}), b (V $decade^{-1}$) is the Tafel slope, and a (V) is the intercept. Exchange current density j_0 (A cm^{-2}) can be determined by the equation:

$$a = (2.3RT)/(\alpha_c F) \times \log j_0 \quad (1)$$

The cathodic transfer coefficient, α_c, can be obtained from the Tafel slope using the equation (2):

$$b = -(2.3RT)/(\alpha_c F) \quad (2)$$

where R (= 8.314 J mol^{-1} K^{-1}) and F (=96,485 C mol^{-1}) are the gas and the Faraday constants, respectively.

The apparent kinetic parameters obtained as have been explained above are collected in Table 3. As it can be observed, Tafel slope and exchange current density increase with the temperature, however at 80 ºC, NiMo1 and NiMo2 electrodes suffer a decrease in these parameters. This fact could be due to at this temperature, HER is more vigorous and the hydrogen bubbles can block the pores of the electrode structure, diminishing the

catalytic activity of the electrodes. The linear regression fitting of the Tafel polarization curves recorded at 30 ºC and 80 ºC showed in Figure 3.a, which allow to calculate the apparent kinetic parameters, are collected in Table 4. As it can be observed, the R^2 values demonstrate that the fits are goods and the Tafel slope and exchange current density have been determined with high precision.

According to the literature of HER on transition metals [10,11,19] and the kinetic parameters obtained (Tafel slopes, b, ranging from 0.113 V dec^{-1} to 0.137 V dec^{-1} at 30 ºC, and cathodic transfer coefficient, α_c, close to 0.5) we can conclude that the HER on the developed electrocatalysts takes place via the Volmer-Heyrovsky mechanism.

Table 3 includes the overpotentials at a fixed current density of -100 mA cm^{-2}, η_{100}. This parameter is a good indicator of the amount of energy required to produce a fixed amount of hydrogen. In order to better compare the values of this parameter for the developed electrodes, the obtained values have been plotted in Fig. 3b. From this Figure is shown that the Ni-Mo electrodes exhibit a better catalytic behaviour than the Ni electrode.

The obtained kinetic parameters, η_{100} and j_0 are quite similar to those obtained by Kubisztal et al. [52] for a NiMo coating with a higher wt.% Mo but lower roughness factor. Fan and Piron [23] also obtained similar η_{100} values for a Ni-Mo electrocatalyst with a comparable wt.% Mo but with far lower j_0 and r_f.

Another good parameter to assess the catalytic activity is the apparent activation energy (E_a) at equilibrium potential [53]. The lower the activation energy, the lower the energy requirements for hydrogen production. The exchange current density is related to the activation energy by the Arrhenius law as show the following equation [54]:

$$\log j_0 = A' - \frac{E_a}{2.303 \cdot R} \cdot \frac{1}{T} \quad (3)$$

where A' (A cm^{-2}) is the pre-exponential factor.

Representing $log\ j_0$ vs $1/T$, a straight line is obtained, the slope from which the activation energy can be calculated. Table 4 collects the linear regression obtained from the Arrhenius plot with the corresponding R-squared, who indicates the goodness of the fit. This table also includes the activation energy values obtained from the slope of the linear regression equation. From these values we easily observe that the electrode NiMo2 exhibits a significant improvement in the catalytic activity for HER, since the activation energy value for this electrocatalyst is reduced to half respect the Ni electrode. The E_a value obtained for the nickel electrode is very similar to the value obtained by other authors when HER takes place via Volmer-Heyrovsky mechanism [17,54-57] and the same occurs with the NiMo electrodes [58].

3.3. Electrochemical impedance spectroscopy measurements

Both, an increase in the electrode surface area and changes in the electrode composition can improve the catalytic activity of the cathodes for HER. In order to distinguish between both effects, two different concepts can be defined: the apparent catalytic activity, based on the surface area and the intrinsic catalytic activity, based on the effective surface area. The parameters obtained above from the polarization measurements are based on the geometric area of the electrodes, so we can concluded about the overall catalytic activity, but not differentiate about the effect of the surface area and the composition of the electrode.

In order to distinguish between the intrinsic and the apparent catalytic activity of an electrode, the effective surface area of the electrode must be calculated. This effective surface area is proportional to the double layer capacitance, which refers to two layers of charges, which behaves like a capacitor [59]. A concept of *Roughness*

factor, R_f, which is the ratio between the real active surface area and the geometrical area of the electrode or what is the same, the ratio between the double layer capacitance of a rough electrode surface and the double layer capacitance of a smooth electrode surface, is employed to quantify the surface area participating in electrode reaction [60].

To obtain the double layer capacitance, the EIS technique is widely employed [14,16,59], by using an equivalent circuit to fit the impedance of an electrode reaction and estimate the electric parameters.

Figure 4 shows the EIS response on the developed electrocatalysts by means of the Nyquist (Fig. 4a) and Bode (Fig. 4b) diagrams. The EIS spectra for the Ni electrode reveals the presence of two strongly overlapped semicircles related to two time constants. However, in the impedance data of NiMo1 and NiMo2 electrodes it can be observed two deformed semicircles clearly differentiated and two maximums in the Bode representation, it is a two-time constants system. As it can be seen from Fig. 4, the diameter of both semicircles diminishes with the overpotencial applied and the same behaviour is observed with the temperature. This fact implies that both time constants are related to the kinetics. This response has been correctly modeled with the equivalent circuit of Fig. 5a. This circuit, initially proposed by Armstrong and Henderson, models the EIS response of a system formed by two semicircles, one at high frequencies, related to the charge transfer and the low frequency semicircle associated with hydrogen adsorption.

When the overpotential applied is too high, the HER is more vigorous and it is difficult to obtain a good EIS spectra, so only one deformed semicircle is observed, it is one-time constant system. In these cases a classical Randles EEC model in which the double layer capacitance was replaced by a constant phase element (CPE) (Fig. 5b) was employed.

In the EIS spectra of all the developed electrocatalyts, at high frequencies, before the formation of the first semicircle, a straight line is observed. This behaviour is independent of the overpotential applied and the same occurs with the temperature, so it is related to the geometry of pores in the electrode surface. The modeling of the impedance response of porous electrodes has been well developed, due to the importance of these materials in electrocatalysis. Keyser et al. [61] studied the impedance response of materials with different pore geometries in absence of faradic reaction. Figure 6 shows the Nyquist diagram which summarizes the behavior at high frequencies associated with the porosity of the material, on the most common pore geometries. Electrodes with cylindrical pores (1) show a 45° straight line at high frequencies in the complex plane representation, while the wedge-shaped porous electrodes (5) have a linear behavior with slopes up to 45°. When the electrodes have the shapes (2), (3) or (4) the complex plane impedance at high frequencies reveals a partial or fully semicircle. Although Keyser et al. [61] studies are performed in absence of electrochemical reaction (only ohmic drop), this EIS response of the pores at high frequencies has been experimentally evidenced and patterned on porous electrodes under HER [13,62].

As an example, in Fig. 6, the experimental impedance spectra recorded on the electrode Ni at 0 mV and 50 °C has been overlapped with the H. Keyser et al. Figure of the EIS spectra on different porous electrodes. As can be seen, the experimental EIS spectra of Ni electrode coincides with the obtained by Keyser for wedge-shaped pores. The same porous shape has been obtained for the NiMo electrodes.

In order to obtain the effective surface area of the developed electrocatalysts, the roughness factor has been calculated by means of the double layer capacitances obtained with the Brug equation [63]:

$$C_{dl} = [Q_1 / (R_S{}^{-1} + R_1{}^{-1})^{(1-n_1)}]^{1/n_1} \quad (4)$$

Table 5 reports the EEC parameters obtained by fitting the experimental data to the equivalent circuit with the software Zview® and the calculated C_{dl} values. The surface roughness factor (R_f) has also been included in Table 5, determined by means of the quotient between the C_{dl} of porous and smooth electrodes [60,64], which approximates to 20 μF cm^{-2} [12,13]. The R_f values are up to 1200, indicating that the effective surface area is far bigger than the geometric area. These R_f values are in the same magnitude order than those reported in literature for electrodeposited Raney Ni-Zn [65], pressed powder Raney Ni-Zn [13], and thermal arc sprayed porous Ni cathodes [66]. Among the developed electrocatalyts, the NiMo2 electrode shows the highest R_f values, so this is the electrode with the highest apparent catalytic activity.

With the R_f values, the effective surface area can be calculated using the relation $A' = A \cdot R_f$, where A' is the effective surface area and A is the geometric area. Then, current density based on the effective surface area can be determined as $j' = i / A'$, which allows to evaluate the intrinsic catalytic activity. Figure 7 shows the Tafel curves of the developed electrocatalysts with respect to j'. As it can be observed from Fig. 7, the Tafel curves corrected to respect the effective surface area for both NiMo electrodes at 80 ºC are collapsed, indicating that both electrodes have the same behaviour at these conditions. The intrinsic kinetic parameters: Tafel slope, exchange current density and cathodic transfer coefficient; obtained from the linear Tafel polarization curves corrected with respect the roughness factor showed on Fig.7 are collected in Table 7. As it can be observed, the Tafel slope and cathodic transfer coefficient are in the same order of magnitude that those obtained with the apparent polarization curves, indicating that the same suggestion that the HER on the developed electrodes takes place via Volmer-Heyrovsky mechanism.

In order to better conclude about the intrinsic catalytic activity of the investigated electrocatalysts, the activation energy based on the effective surface area (intrinsic activation energy, E_a') can be calculated from the exchange current densities corrected with the obtained R_f values, j_0'. The E_a' values and the corresponding linear regression expression have been collected on Table 6. As it shown, the NiMo electrodes have higher intrinsic catalytic activity than the Ni electrode because its activation energy has been reduced to half. Both NiMo electrodes have similar E_a' values, so similar intrinsic activity. This improvement in the intrinsic catalytic activity could be a consequence of the synergetic effect of the hypo-hyper-d-electronic transition metals alloy on hydrogen evolution [15-16].

4. Conclusions

3D macroporous Ni and NiMo cathodes have been developed and characterized both morphological and electrochemically for hydrogen evolution reaction (HER) in 30 wt.% KOH solution. The cathodes were synthesized via a double-template electrochemical process. The typical three-dimensional metal foam structure with dendritic walls was obtained.

From the electrochemical study it can be concluded that by alloying Nickel with Molybdenum it is possible improve the apparent and the intrinsic catalytic activity for HER. The activation energy values have been calculated from the exchange current densities. The results of this parameter and both the apparent and intrinsic kinetic parameters indicate that the HER on these electrodes takes place via Volmer-Heyrovsky mechanism.

EIS results allow us to conclude about the effective surface area which is related to the apparent catalytic activity and allow us also to conclude about the porous shape. The developed electrodes present a wedge-shaped pores according to the Keyser et. al studies. Combining EIS and Tafel results it also can be shown that the NiMo electrodes have higher intrinsic catalytic activity than the Ni electrode regardless of the atomic percentage of Mo in the alloy.

Acknowledgements

The authors acknowledge the support of Generalitat Valenciana (PROMETEO/2010/023) and Universidad Politécnica de Valencia (PAID-06-10-2227).

REFERENCES

[1] Verizoglu TN, Sherif SA, Barbir F (2005) Hydrogen energy solutions. In: Agardy FJ and Nemerow NL (Eds) Enviromental Solutions, Elsevier Inc., USA, pp 143-180

[2] Barbir F (2009) Transition to renewable energy systems with hydrogen as an energy carrier. Energy 34:308-312. doi: 10.1016/j.energy.2008.07.007

[3] Veziroglu TN, Barbir F (1992) Hydrogen: the wonder fuel. Int J Hydrogen Energy 17:391-404. doi: 10.1016/0360-3199(92)90183-W

[4] Zeng K, Zhang D (2010) Recent progress in alkaline water electrolysis for hydrogen production and applications. Progr Energy Combust 36:307-326. doi: 10.1016/j.pecs.2009.11.002

[5] Stojić DLj, Marĉeta MP, Sovilj SP, Miljanić SS (2003) Hydrogen generation from water electrolysis—possibilities of energy saving. J Power Sources 118:315-319. doi: 10.1016/S0378-7753(03)00077-6

[6] Souza RF, Padilha JC, Gonçalves RS, Souza MO, Rault-Berthelot J (2007) Electrochemical hydrogen production from water electrolysis using ionic liquid as electrolytes: Towards the best device, J Power Sources 164:792-798. doi: 10.1016/j.jpowsour.2006.11.049

[7] Stojić DLj, Grozdić TD, Kaninski MPM, Maksić AD, Simić ND (2006) Intermetallics as advanced cathode materials in hydrogen production via electrolysis. Int J Hydrogen Energy 31:841-846. doi: 10.1016/j.ijhydene.2005.08.009

[8] Yazici B, Tatli G, Galip H, Erbil M (1995) Investigation of suitable cathodes for the production of hydrogen gas by electrolysis. Int J Hydrogen Energy 20:957-965. doi: 10.1016/0360-3199(95)00032-9

[9] Solmaz R, Kardaş G (2011) Fabrication and characterization of NiCoZn–*M* (*M*: Ag, Pd and Pt) electrocatalysts as cathode materials for electrochemical hydrogen production. Int J Hydrogen Energy 36:12079-12087. doi: 10.1016/j.ijhydene.2011.06.101

[10] Lasia A (2003) Hydrogen evolution reaction. In: Vielstich W, Lamm A, Gasteiger HA (Eds) Handbook of fuel cells: fundamentals, technology and applications. Volume 2: Fuel cell electrocatalysis, John Wiley and Sons Ltd, pp 416-440

[11] Lasia A, Rami A (1990) Kinetics of hydrogen evolution on nickel electrodes. J Electroanal Chem Interfacial Electrochem 294:123-141. doi: 10.1016/0022-0728(90)87140-F

[12] Rami A, Lasia A (1992) Kinetics of hydrogen evolution on Ni-Al alloy electrodes. J Appl Electrochem 22:376-382. doi: 10.1007/BF01092692

[13] Chen LL, Lasia A (1992) Study of the kinetics of hydrogen evolution reaction on Nickel-Zinc powder electrodes. J Electrochem Soc 139:3214-3219. doi: 10.1149/1.2069055

[14] Herraiz-Cardona I, Ortega E, García-Antón J, Pérez-Herranz V (2011) Assessment of the roughness factor effect and the intrinsic catalytic activity for hydrogen evolution reaction on Ni-based electrodeposits. Int J Hydrogen Energy 36:9428-9438. doi: 10.1016/j.ijhydene.2011.05.047

[15] Lupi C, Dell'Era A, Pasquali M (2009) Nickel–cobalt electrodeposited alloys for hydrogen evolution in alkaline media. Int. J. Hydrogen Energy 34:2101-2106. doi:10.1016/j.ijhydene.2009.01.015

[16] Herraiz-Cardona I, Ortega E, Pérez-Herranz V (2011) Impedance study of hydrogen evolution on Ni/Zn and Ni–Co/Zn stainless steel based electrodeposits. Electrochim Acta 56:1308-1315. doi: 10.1016/j.electacta.2010.10.093

[17] Herraiz-Cardona I, González-Buch C, Valero-Vidal C, Ortega E, Pérez-Herranz V (2013) Co-modification of Ni-based type Raney electrodeposits for hydrogen evolution reaction in alkaline media. J Power Sources 240:698-704. doi: 10.1016/j.jpowsour.2013.05.041

[18] Herraiz-Cardona I, Ortega E, Vázquez-Gómez L, Pérez-Herranz V (2011) Electrochemical characterization of a NiCo/Zn cathode for hydrogen generation. Int J Hydrogen Energy 36:11578-11587. doi: 10.1016/j.ijhydene.2011.06.067

[19] Navarro-Flores E, Chong Z, Omanovic S (2005) Characterization of Ni, NiMo, NiW and NiFe electroactive coatings as electrocatalysts for hydrogen evolution in an acidic medium. J Mol Catal A-Chem 226:179-197. doi: 10.1016/j.molcata.2004.10.029

[20] Giz MJ, Benito SC, González ER (2000) NiFeZn codeposited as a cathode material for the production of hydrogen by water. Int J Hydrogen Energy 25:621-626. doi:10.1016/S0360-3199(99)00084-1

[21] Solmaz R, Kardaş G (2009) Electrochemical deposition and characterization of NiFe coatings as electrocatalytic materials for alkaline water electrolysis. Electrochim Acta 54:3726-3734. doi:10.1016/j.electacta.2009.01.064

[22] Ullal Y, Hegde AC (2014) Electrodeposition and electro-catalytic study of nanocrystalline Ni-Fe alloy. Int J Hydrogen Energy 39:10485-10492. doi:10.1016/j.ijhydene.2014.05.016

[23] Fan C, Piron DL, Sleb A, Paradis P (1994) Study of Electrodeposited Nickel-Molybdenum, Nickel-Tungsten, Cobalt-Molybdenum, and Cobalt-Tungsten as Hydrogen Electrodes in Alkaline Water Electrolysis. J Electrochem Soc 141:382-387. doi: 10.1149/1.2054736

[24] Solmaz R, Döner A, Kardaş G (2009) The stability of hydrogen evolution activity and corrosion behavior of NiCu coatings with long-term electrolysis in alkaline solution. Int J Hydrogen Energy 34:2089-2094. doi:10.1016/j.ijhydene.2009.01.007

[25] Wu L, He Y, Lei T, Nan B, Xu N, Zou J, Huang B, Liu CT (2014) The stability of hydrogen evolution activity and corrosion behavior of porous Ni_3Al–Mo electrode in alkaline solution during long-term electrolysis. Energy 67:19-26. doi: 10.1016/j.energy.2014.02.033

[26] Sheela G, Pushpavanam M, Pushpavanam S (2002) Zinc–nickel alloy electrodeposits for water electrolysis. Int J Hydrogen Energy 27:627-633. doi:10.1016/S0360-3199(01)00170-7

[27] Solmaz R, Kardaş G (2007) Hydrogen evolution and corrosion performance of NiZn coatings. Energ Convers Manage 48 (2007) 583-591. doi:10.1016/j.enconman.2006.06.004

[28] Brewer (1963). In: Beck PA (Ed) Electronic structure and alloy chemistry of transition elements, Interscience, New York, p 221

[29] Jaksic MM (1984) Electrocatalysis of hydrogen evolution in the light of the brewer—engel theory for bonding in metals and intermetallic phases. Electrochim Acta 29:1539-1550. doi:10.1016/0013-4686(84)85007-0

[30] Jaksic MM, Jaksic JM (1984) Fermi dynamics and some structural bonding aspects of electrocatalysis for hydrogen evolution**.** Electrochim Acta 39: 1695-1714. doi:10.1016/0013-4686(94)85155-7

[31] Jaksic MM, Lacnjevac CM, Grgur BN, Krstajic NV (2000) Volcano plots along intermetallic hypo-hyper-d-electronic phase diagrams and electrocatalysis for hydrogen electrode reactions. J New Mat Electrochem Systems 3:131-144

[32] Jaksic MM (2001) Hypo–hyper-d-electronic interactive nature of interionic synergism in catalysis and electrocatalysis for hydrogen reactions. Int J Hydrogen Energy 26:559-578. doi: 10.1016/S0360-3199(00)00120-8

[33] Raj IA, Venkatesan VK (1988) Characterization of nickel-molybdenum and nickel-molybdenum-iron alloy coatings as cathodes for alkaline water electrolysers. Int J Hydrogen Energy 13:215-223. doi: 10.1016/0360-3199(88)90088-2

[34] Gennero de Chialvo MR, Chialvo AC (1998) Hydrogen evolution reaction on smooth Ni(1−x)+Mo(x) alloys ($0 \leq x \leq 0.25$). J Electroanal Chem 448:87-93. doi: 10.1016/S0022-0728(98)00011-4

[35] Simpraga R, Bai L, Conway BE (1995) Real area and electrocatalysis factors in hydrogen evolution kinetics at electrodeposited Ni-Mo and Ni-Mo-Cd composites: effect of Cd content and nature of substrate. J Appl Electrochem 25:628-641. doi: 10.1007/BF00241924

[36] Fan C, Piron DL, Paradis P (1994) Hydrogen evolution on electrodeposited nickel-cobalt-molybdenum in alkaline water electrolysis. Electrochim Acta 39:2715-2722. doi: 10.1016/0013-4686(94)00263-0

[37] Raj IA, Vasu KI (1990) Transition metal-based hydrogen electrodes in alkaline solution−electrocatalysis on nickel based binary alloy coatings. J Appl Electrochem 20:32-38. doi: 10.1007/BF01012468

[38] Raj IA, Vasu KI (1992) Transition metal-based cathodes for hydrogen evolution in alkaline solution: Electrocatalysis on nickel-based ternary electrolytic codeposits. J Appl Electrochem 22:471-477. doi: 10.1007/BF01077551

[39] Divisek J, Schmitz H, Balej J (1989) Ni and Mo coatings as hydrogen cathodes. J Appl Electrochem 19:519-530. doi: 10.1007/BF01022108

[40] Huot JY, Trudeau ML, Schulz R (1991) Low Hydrogen Overpotential Nanocrystalline Ni‐Mo Cathodes for Alkaline Water Electrolysis. J Electrochem Soc 138:1316-1321. doi: 10.1149/1.2085778

[41] Krstajić NV, Jović VD, Gajić-Krstajić Lj, Jović BM, Antozzi AL, Martelli GN (2008) Electrodeposition of Ni–Mo alloy coatings and their characterization as cathodes for hydrogen evolution in sodium hydroxide solution. Int J Hydrogen Energy 33:3676-3687. doi: 10.1016/j.ijhydene.2008.04.039

[42] Dini JW (1993) Electrodeposition: the materials science of coating and substances. Noyes Publications, New Jersey

[43] D. Wood. Metal Industry 36 (1938) 330.

[44] Herraiz-Cardona I, Ortega E, Vázquez-Gómez L, Pérez-Herranz V (2012) Double-template fabrication of three-dimensional porous nickel electrodes for hydrogen

evolution reaction. Int J Hydrogen Energy 37:2147-2156. doi: 10.1016/j.ijhydene.2011.09.155

[45] Herraiz-Cardona I, González-Buch C, Ortega E, García-Antón J, Pérez-Herranz (2013) Energy efficiency improvement of alkaline water electrolysis by using 3D Ni cathodes fabricated via a double-template electrochemical process. Chem Eng Trans 32: 451-456. doi: 10.3303/CET1332076

[46] Shin H, Liu M (2004) Copper Foam Structures with Highly Porous Nanostructured Walls. Chem Mater 16:5460-5464. doi: 10.1021/cm048887b

[47] Bonou L, Eyraud M, Denoyel R, Massiani Y (2002) Influence of additives on Cu electrodeposition mechanisms in acid solution: direct current study supported by non-electrochemical measurements. Electrochim Acta 47:4139-4148. doi: 10.1016/S0013-4686(02)00356-0

[48] Nagy Z, Blaudeau JP, Hung NC, Curtiss LA, Zurawski DJ (1995) Chloride Ion Catalysis of the Copper Deposition Reaction. J Electrochem Soc 142:L87-L89. doi: 10.1149/1.2044254

[49] Soares DM, Wasle S, Weil KG, Doblhofer K (2002) Chloride Ion Catalysis of the Copper Deposition Reaction. J Electroanal Chem 532:353-358. doi: 0.1149/1.2044254

[50] Halim J, Abdel-Karim R, El-Raghy S, Nabil M, Waheed A (2012) Electrodeposition and Characterization of Nanocrystalline Ni-Mo Catalysts for Hydrogen Production. Journal of nanomaterials 2012:9. doi:10.1155/2012/845673

[51] García-Antón J, Igual-Muñoz A, Guiñón JL, Pérez-Herranz V (2000) Horizontal Electrochemical Cell by the Electro-Optical Analysis of Electrochemical Process. Spain P-200002526

[52] Kubisztal J, Budniok A, Lasia A (2007) Study of the hydrogen evolution reaction on nickel-based composite coatings containing molybdenum powder. Int J Hydrogen Energy 32:1211-1218.

[53] Jukic A, Piljac J, Meticoš-Hukovic M (2001) Electrocatalytic behavior of the $Co_{33}Zr_{67}$ metallic glass for hydrogen evolution. J Mol Catal A-Chem 166:293-302. doi: 10.1016/S1381-1169(00)00452-0

[54] Savadogo O, Ndzebet E (2001) Influence of $SiW_{12}O_{40}^{4-}$ on the electrocatalytic behaviour of Pt–Co alloy supported on carbon for water electrolysis in 3 M KOH aqueous solution. Int J Hydrogen Energy 26:213-218. doi: 10.1016/S0360-3199(00)00059-8

[55] Correia AN, Machado SAS (1998) Hydrogen evolution on electrodeposited Ni and Hg ultramicroelectrodes. Electrochim Acta 43:367-373. doi: 10.1016/S0013-4686(97)00050-9

[56] Machado SAS, Avaca LA (1994) The hydrogen evolution reaction on nickel surfaces stabilized by H-absorption. Electrochim Acta 39:1385-1391. doi: 10.1016/0013-4686(94)E0003-I

[57] Tie-chui Y, Rui-di L, Ke-chao Z (2004) Electrocatalytic properties of Ni-S-Co coating electrode for hydrogen evolution in alkaline medium**.** Trans Nonferrous Metals Soc China 17:762-765. 10.1016/S1003-6326(07)60170-8

[58] Tasic GS, Maslovara SP, Zugic DL, Maksic AD, Kaninski MPM (2011) Characterization of the Ni–Mo catalyst formed *in situ* during hydrogen generation from alkaline water electrolysis. Int J Hydrogen Energy 36:11588-11595. doi: 10.1016/j.ijhydene.2011.06.081

[59] Bard AJ, Inzelt G, Scholz F (2008) Electrochemical dictionary, 1st Edition. Springer, Berlin

[60] Zeng K, Zhang D (2014) Evaluating the effect of surface modifications on Ni based electrodes for alkaline water electrolysis. Fuel 116:692-698. doi: 10.1016/j.fuel.2013.08.070

[61] Keyser H, Beccu KD, Gutjahr MA (1976) Abschätzung der porenstruktur poröser elektroden aus impedanzmessungen. Electrochim Acta 21:539-543. doi: 0.1016/0013-4686(76)85147-X

[62] Levie R (1967) Electrochemical responses of porous and rough electrodes. In Delahay P (ed) Advances in electrochemistry and electrochemical engineering, Vol. 6, Interscience, New York, pp. 329-397

[63] Brug GJ, Van den eeden ALG, Sluyters-rehbach M, Sluyters JH (1984) The analysis of electrode impedances complicated by the presence of a constant phase element. J Electroanal Chem 176:275-295

[64] Trasatti S, Petrii OA (1991) Real surface area measurements in electrochemistry. Pure & Appl Chem 63:711-734. doi : 10.1351/pac199163050711

[65] Chen L, Lasia A (1991) Study of the Kinetics of Hydrogen Evolution Reaction on Nickel‐Zinc Alloy Electrodes. J Electrochem Soc 138:3321-3328. doi: 10.1149/1.2085409

[66] Kellenberger A, Vaszilcsin N, Brandl W, Duteanu N (2007**)** Kinetics of hydrogen evolution reaction on skeleton nickel and nickel–titanium electrodes obtained by

thermal arc spraying technique. Int J Hydrogen Energy 32:3258-3265. doi: 10.1016/j.ijhydene.2007.02.028

LIST OF TABLES

LIST OF FIGURES

Table 1 Bath compositions and operating conditions used to obtain 3D macroporous electrodes

Electrode	Bath Composition (M)				Operating Conditions			
	Cu Template		Ni/NiMo Electrodeposition		Cu Template		Ni/NiMo Electrodeposition	
Ni	$CuSO_4$	0.05	$NiSO_4$	1.26	T (ºC)	25	T (ºC)	50
	H_2SO_4	0.50	$NiCl_2$	0.19	j_d (A cm^{-2})	0.10	j_d (A cm^{-2})	0.05
	HCl	0.01	H_3BO_3	0.60	Time (s)	450	Time (s)	3600
NiMo1	$CuSO_4$	0.05	$NiSO_4$	0.20	T (ºC)	25	T (ºC)	25
			Na_2MoO_4	0.02	j_d (A cm^{-2})	0.10	j_d (A cm^{-2})	0.04
	H_2SO_4	0.50	$Na_3C_6H_5O_7$	0.30	Time (s)	450	Time (s)	1800
			NH_4OH	Excess	pH	0.5	pH	9.5
NiMo2	$CuSO_4$	0.05	$NiSO_4$	0.20	T (ºC)	25	T (ºC)	25
			Na_2MoO_4	0.02	j_d (A cm^{-2})	0.10	j_d (A cm^{-2})	0.04
	H_2SO_4	0.50	$Na_3C_6H_5O_7$	0.30	Time (s)	450	Time (s)	3600
			NH_4OH	Excess	pH	0.5	pH	9.5

Table 2 Composition of the investigated electrocatalytic coatings in at.%

Catalyst	Ni	Mo
Ni	100.0	-
NiMo1	96.1	3.9
NiMo2	85.7	14.3

Table 3 Apparent kinetic parameters of the HER obtained from the polarization curves recorded in 30 wt.% KOH solution at different temperatures

Catalyst	Temperature (ºC)					
	30	**40**	**50**	**60**	**70**	**80**
Ni						
b **(mV dec^{-1})**	96.3	98.0	101.7	105.2	108.7	114.5
j_0 **(mA cm^{-2})**	0.38	0.40	0.57	0.73	0.94	1.11
α_c	0.62	0.63	0.63	0.63	0.63	0.61
η_{100}	230	234	227	223	220	226
NiMo1						
b **(mV dec^{-1})**	136.0	146.2	159.0	170.8	181.6	152.6
j_0 **(mA cm^{-2})**	2.64	5.48	9.84	16.99	27.51	8.05
α_c	0.44	0.42	0.40	0.39	0.37	0.46
η_{100}	216	185	160	132	104	125
NiMo2						
b **(mV dec^{-1})**	129.0	125.0	135.6	139.4	146.5	147.6
j_0 **(mA cm^{-2})**	6.79	8.05	12.49	14.31	17.33	17.78
α_c	0.47	0.50	0.47	0.47	0.46	0.47
η_{100}	151	137	123	117	111	149

Table 4 Linear regression fitting of the Tafel polarization curves recorded on the investigated electrocatalytic coatings in 30 wt.% KOH solution at 30 and 80 ºC

Catalyst	Linear regression Temperature	
	30	**80**
Ni	$\eta = -0.0963 \cdot \log\|j\| - 0.3293;\ \ R^2 = 0.9976$	$\eta = -0.1145 \cdot \log\|j\| - 0.3385;\ \ R^2 = 0.9941$
NiMo1	$\eta = -0.1360 \cdot \log\|j\| - 0.3506;\ \ R^2 = 0.9995$	$\eta = -0.1526 \cdot \log\|j\| - 0.3196;\ \ R^2 = 0.9998$
NiMo2	$\eta = -0.1290 \cdot \log\|j\| - 0.2797;\ \ R^2 = 0.9992$	$\eta = -0.1476 \cdot \log\|j\| - 0.2583;\ \ R^2 = 0.9994$

Table 5 Apparent activation energy values, E_a (kJ mol^{-1}), of the investigated electrocatalytic coatings in 30 wt.% KOH solution

Catalyst	Linear regression	E_a (kJ mol^{-1})
Ni	$\log j_0 = -2.110 \cdot 10^3 \cdot \frac{1}{T} + 3.831; \quad R^2 = 0.991$	40.4
NiMo1	$\log j_0 = -1.983 \cdot 10^3 \cdot \frac{1}{T} + 4.071; \quad R^2 = 0.863$	38.0
NiMo2	$\log j_0 = -1.077 \cdot 10^3 \cdot \frac{1}{T} + 1.387; \quad R^2 = 0.966$	20.6

Table 6 Surface roughness factors, R_f, determined from the EIS study on the investigated electrocatalytic coatings at 30 wt.% KOH solution at 50ºC

Electrode	|η| (mV)	R_S (Ω cm^2)	R_{ct} (Ω cm^2)	Q_1 (Ω^{-1} cm^{-2}s^n)	n_1	C_{dl} (F cm^{-2})	R_{ads} (Ω cm^2)	Q_2 (Ω^{-1} cm^{-2}s^n)	n_2	C_{ads} (F cm^{-2})	R_f
Ni	0	0.13	14.8	0.084	0.79	0.050	13.8	0.27	0.68	0.10	2481
	51	0.15	8.1	0.061	0.80	0.037	3.9	0.20	0.64	0.07	1866
	100	0.14	3.8	0.061	0.78	0.035	-	-	-	-	1754
	147	0.15	1.5	0.048	0.80	0.029	-	-	-	-	1430
NiMo1	0	0.31	3.42	0.048	0.85	0.038	7.12	0.60	0.75	0.40	1923
	63	0.31	2.52	0.040	0.84	0.031	0.87	1.69	0.71	0.93	1572
	106	0.31	1.55	0.034	0.84	0.029	0.21	5.47	0.70	2.22	1299
	146	0.31	0.81	0.032	0.84	0.024	-	-	-	-	1201
NiMo2	0	0.28	1.36	0.088	0.85	0.067	31.1	0.80	0.80	0.58	3366
	54	0.29	1.10	0.055	0.90	0.047	0.96	1.57	0.73	0.90	2326
	93	0.30	0.78	0.044	0.90	0.037	0.21	2.80	0.80	1.67	1831
	126	0.30	0.46	0.048	0.87	0.037	-	-	-	-	1835

Table 7 Intrinsic kinetic parameters of the HER obtained from the polarization curves recorded in 30 wt.% KOH solution at different temperatures

Catalyst	Temperature (°C)		
	30	50	80
Ni			
b' (mV dec^{-1})	89.0	85.1	91.1
j'_0 (μA cm^{-2})	0.28	0.28	0.32
α'_c	0.61	0.64	0.59
NiMo1			
b' (mV dec^{-1})	119.3	121.8	95.9
j'_0 (μA cm^{-2})	2.29	4.81	5.50
α'_c	0.45	0.44	0.56
NiMo2			
b' (mV dec^{-1})	104.7	114.0	92.7
j'_0 (μA cm^{-2})	1.91	5.54	10.56
α'_c	0.57	0.56	0.76

Table 8 Intrinsic activation energy values, E_a' (kJ mol^{-1}), of the investigated electrocatalytic coatings in 30 wt.% KOH solution

Catalyst	Linear regression	E_a' (kJ mol^{-1})
Ni	$\log j_0 = -3.248 \cdot 10^3 \cdot \frac{1}{T} + 3.663; \quad R^2 = 0.976$	62.2
NiMo1	$\log j_0 = -1.921 \cdot 10^3 \cdot \frac{1}{T} + 0.653; \quad R^2 = 0.857$	36.8
NiMo2	$\log j_0 = -1.798 \cdot 10^3 \cdot \frac{1}{T} + 0.142; \quad R^2 = 0.986$	34.4

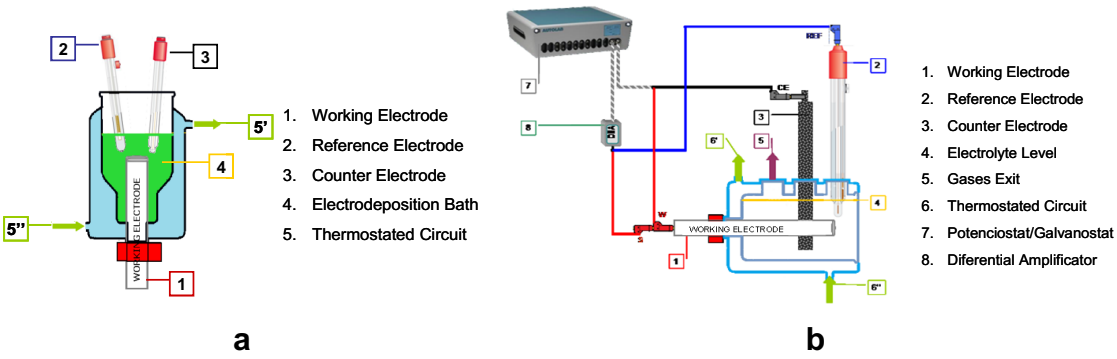

Fig. 1 a Thermostated one-compartmented cell for the electrodeposition process; **b** Electrochemical cell P200002526 for the electrochemical measurements

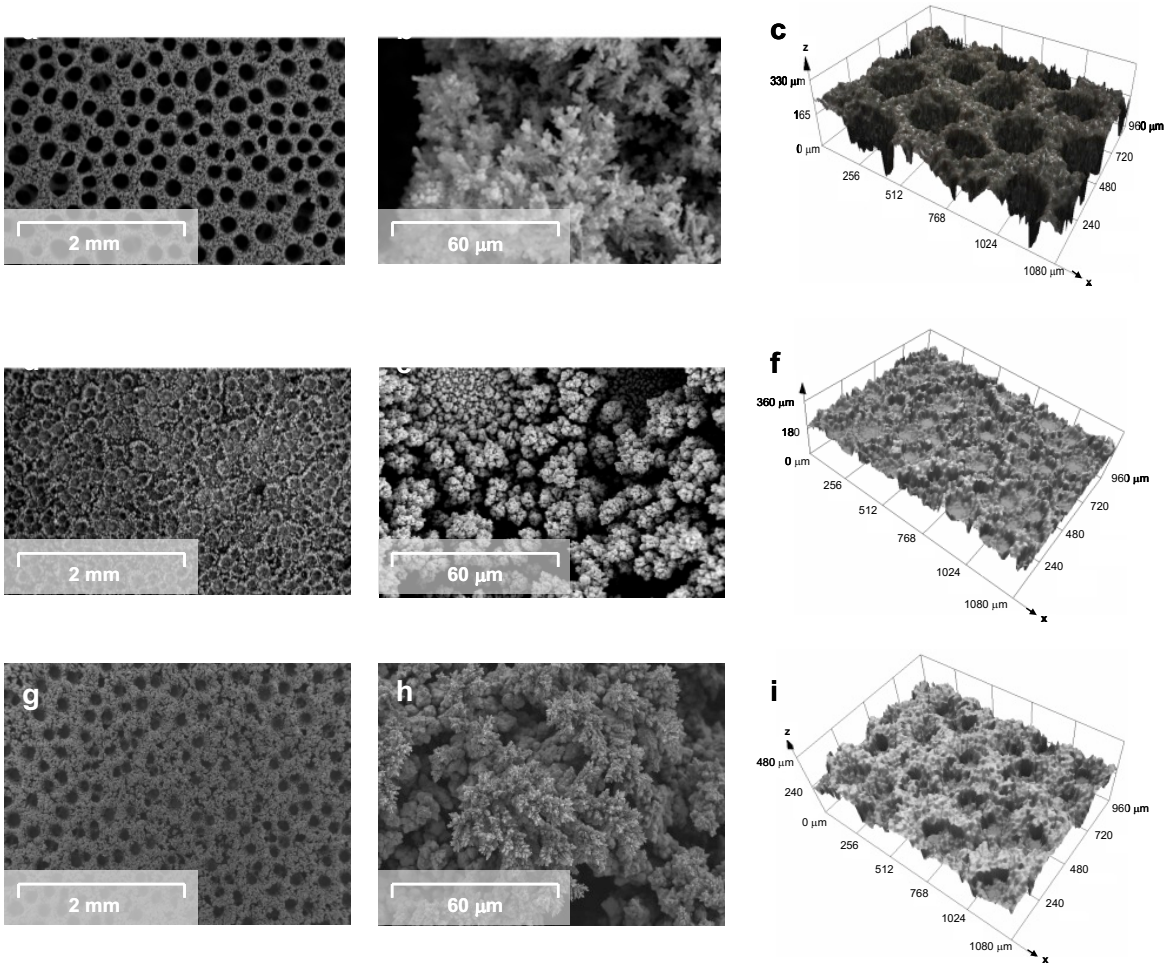

Fig. 2 FE-SEM images and 3D confocal laser micrographs of Ni electrode (**a**, **b**, **c**), NiMo1 electrode (**d**, **e**, **f**) and NiMo2 electrode (**g**, **h**, **i**). Magnification: ×30 (**a**, **d**, **g**), ×1000 (**b**, **e**, **h**) and ×100 (**c**, **f**, **i**)

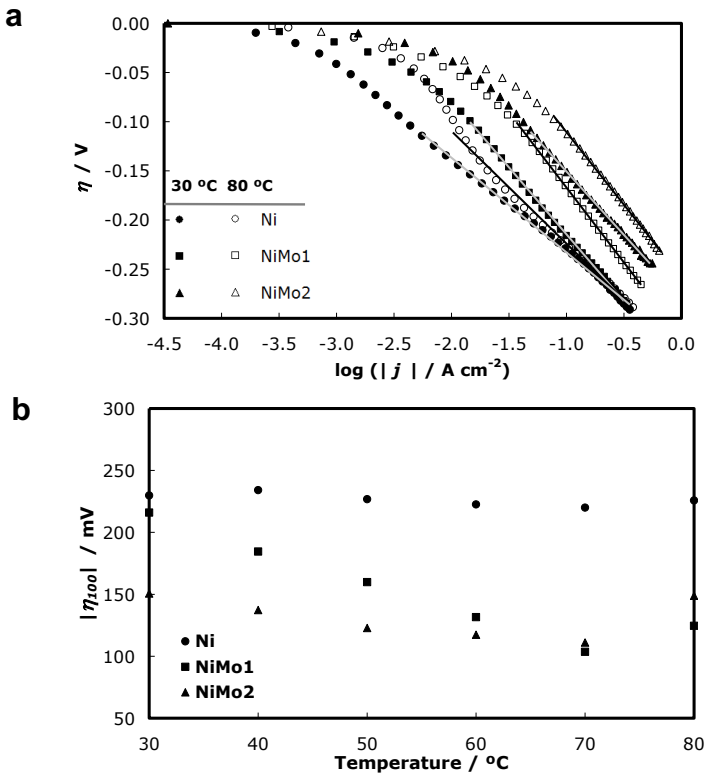

Fig. 3 a Linear Tafel polarization curves recorded on the investigated electrocatalytic coatings in 30 wt.% KOH solution at 30 (filled dots) and 80 ºC (empty dots); **b** overpotentials at a current density of -100 mA·cm^{-2}, η_{100}, recorded on the investigated electrocatalytic coatings in 30 wt.% KOH solution

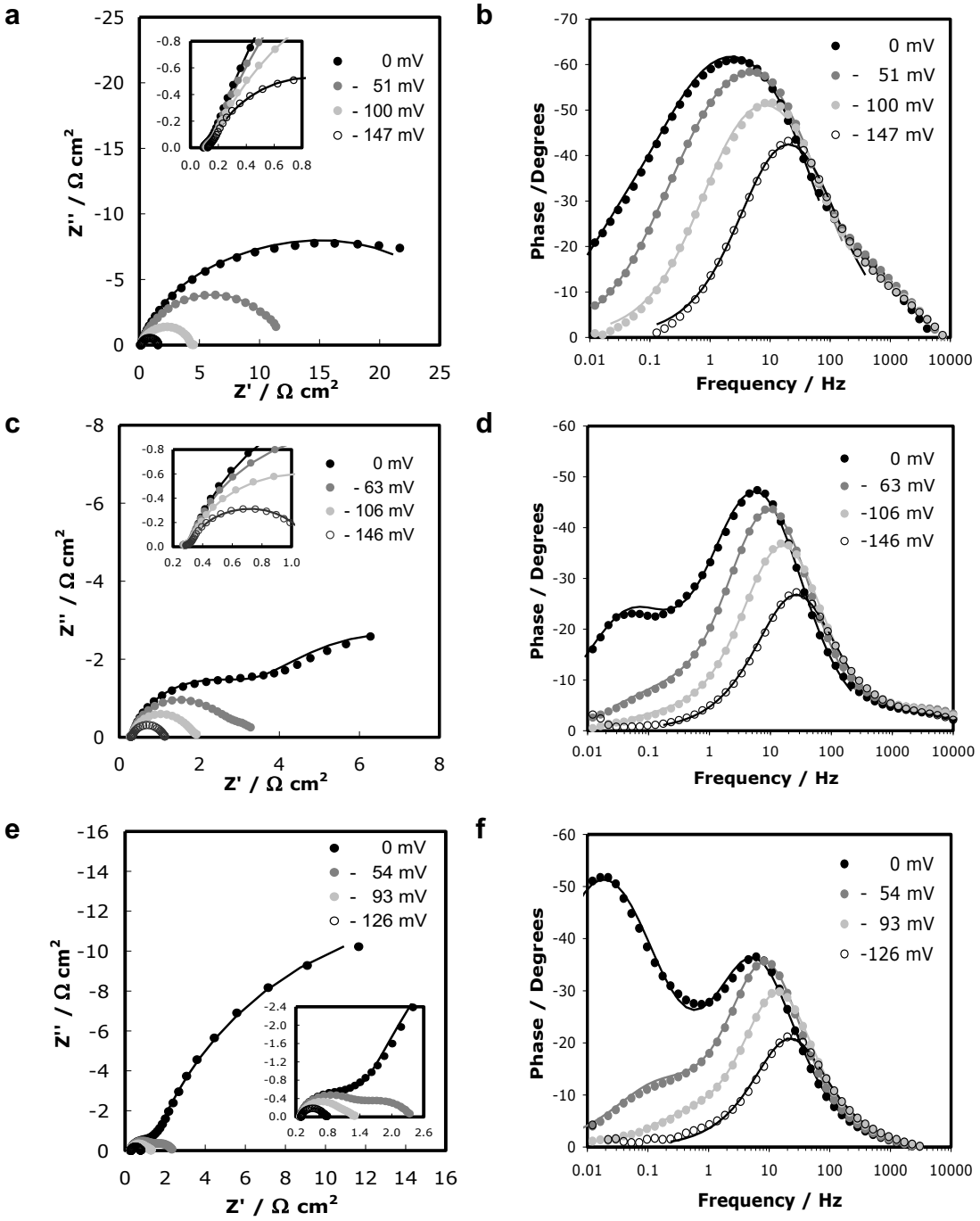

Fig. 4 Impedance data obtained in 30 wt.% KOH solution at 50º C for Ni electrode (**a**, **b**), NiMo1 electrode (**c**, **d**) and NiMo2 electrode (**e**, **f**). Nyquist representation (**a**, **b**, **c**) and Bode representation of the phase angle as a function frequency (**d**, **e**, **f**). Symbols are the experimental points and solid lines are modelled data

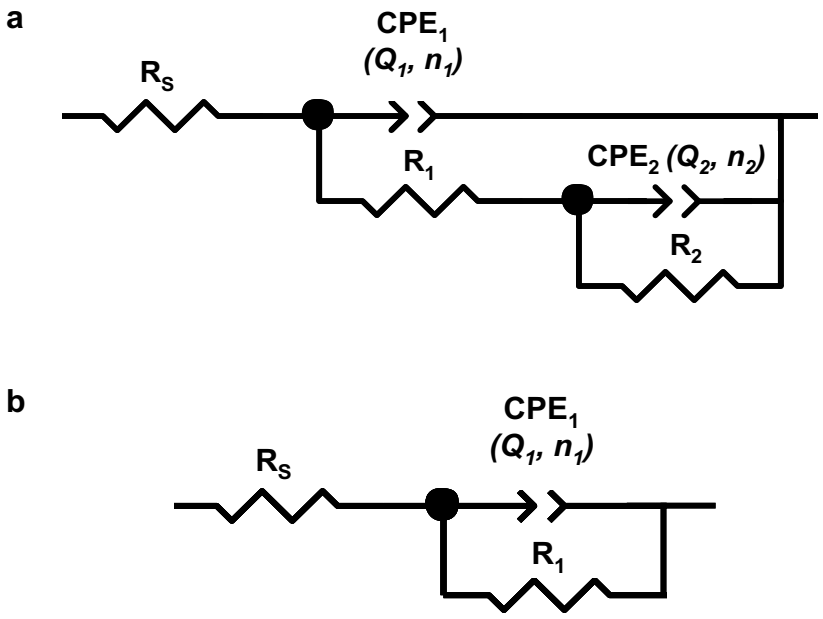

Fig. 5 EEC models used to explain the EIS response of the HER on the developed electrocatalysts: **a** two-time constant parallel model (2TP) and **b** one-time constant (1T)

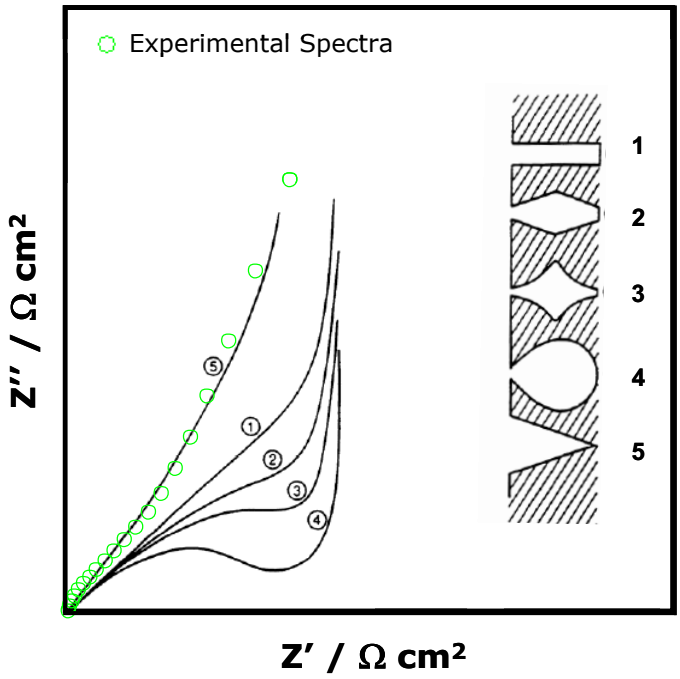

Fig. 6 Schedule of the pore geometry by means the comparison of the experimental spectra with the Nyquist diagram of high frequency impedance spectra in different pore geometry electrodes obtained by Keyser et. al [52]

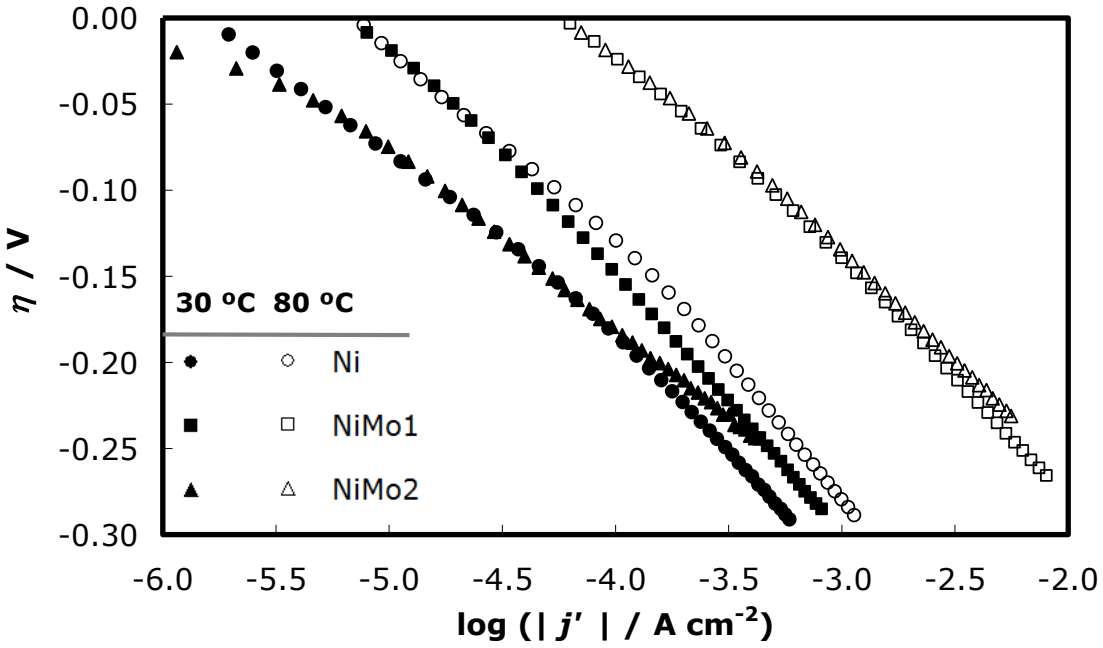

Fig. 7 Linear Tafel polarization curves recorded on the investigated electrocatalytic coatings in 30% wt. KOH solution at 30 (filled dots) and 80 ºC (empty dots), illustrating the intrinsic activity